AIAA JOURNAL
Vol. 37, No. 9, September 1999

New Formulation of Hardin–Pope Equations for Aeroacoustics

John A. Ekaterinaris*
Risoe National Laboratory, DK-4000 Roskilde, Denmark

Predictions of aeroacoustic disturbances generated by low-speed unsteady flows can be obtained with the two-step method proposed by Hardin and Pope (Hardin, J. C., and Pope, S. D., "An Acoustic/Viscous Splitting Technique for Computational Aeroacoustics," *Theoretical and Computational Fluid Dynamics*, Vol. 6, No. 5–6, 1994, pp. 334–340). This method requires detailed information about the unsteady aerodynamic flowfield, which usually is obtained from a computational fluid dynamics solution. A new, conservative formulation of the equations governing acoustic disturbances is presented. The conservative form of the governing equations is obtained after application of a transformation of variables that produces a set of inhomogeneous equations similar to the conservation-law form of the compressible Euler equations. The source term of these equations depends only on the derivatives of the hydrodynamic variables. Explicit time marching is performed. A high-order-accurate, upwind-biased numerical scheme is used for numerical solution of the conservative equations. The convective fluxes are evaluated using upwind-biased formulas and flux-vector splitting. Solutions are obtained for the acoustic flowfield generated by a corotating vortex pair. Computed results are compared with the analytic solution.

Nomenclature

A, B	= flux Jacobian matrices
c	= speed of sound
e	= internal energy
$\boldsymbol{F}, \boldsymbol{G}$	= mixed-type flux vectors
$\boldsymbol{f}, \boldsymbol{g}$	= conservative flux vectors
P	= hydrodynamic pressure
P_o	= freestream pressure
$\bar{P}$	= average pressure
p'	= acoustic pressure
$\boldsymbol{Q}$	= acoustic and flow variable vector
$\boldsymbol{q}$	= conservative variable vector
$\mathcal{R}$	= residual-term vector
R_o	= half distance between point vortices
S	= source term
U, V	= incompressible velocity components
u', v'	= acoustic velocity components
x, y	= Cartesian coordinates
Γ	= vortex circulation
ρ_o	= constant incompressible density
ρ_1	= density correction
ρ'	= acoustic density
ω	= angular velocity

I. Introduction

AERODYNAMIC sound generation by low-speed flows is of interest for many applications, such as automobile and wind turbine noise. Direct numerical simulations (DNSs) of the full compressible equations, which describe both sound generation and propagation, can be used for simple model problems.[1] Aeroacoustic calculations with DNSs for low Mach numbers, however, are prohibitively expensive. Less computationally intensive methods, such as acoustic analogies[2] or numerical solution of the linearized Euler equations,[3,4] can be used for sound propagation. These methods, however, require information about the character and strength of the sound sources. In Ref. 2, noise generation from laminar, low-speed flow over an airfoil at an angle of attack was computed using an integral formulation of Lighthill's[5] acoustic analogy. The acoustic dipole and quadrupole sources[2] were obtained from a Navier–Stokes solution. In Ref. 4, the sound radiation from a monopole source in the presence of a uniform stream was computed. The far-field sound radiation also can be obtained from a Kirchoff method. Kirchoff methods[6] are applied in connection with a computational fluid dynamics (CFD) solution that is used to compute pressure variations on a closed surface. The accuracy of the predicted far-field acoustic intensity depends on the accuracy of the computed time-dependent pressure distribution on this surface.

Recently, Hardin and Pope[7] introduced a two-step approach suitable for the computation of sound generated by low-speed, unsteady flows. This method utilizes information for the entire incompressible flowfield, which is obtained from a CFD computation or a closed-form expression. The incompressible field solution is used to define a density perturbation ρ_1 and to split the compressible Euler equations into hydrodynamic terms and perturbed acoustic terms. The computation of sound generation and propagation is carried out in two steps as follows: First, the time-dependent velocities and pressure of the viscous, incompressible flowfield are obtained either from a closed-form solution or from a numerical solution of the unsteady, incompressible-flow equations. Next, the acoustic radiation is obtained from the numerical solution of a set of inhomogeneous, inviscid equations. These equations include the variable-density perturbation ρ_1, which relates the incompressible flowfield to the acoustic disturbances. The incompressible density correction ρ_1 acts as the sound source to the compressible acoustic field. This density is defined as the deviation of the instantaneous pressure from its average value via isentropic relations. Furthermore, other hydrodynamic quantities, such as velocities and pressure, multiply the acoustic perturbations or appear as source terms in the equation that governs aeroacoustic disturbances, and couple hydrodynamic variations to the acoustic field. The advantage of the two-step method of Hardin and Pope is that it makes possible computation of aeroacoustic noise generation and propagation by viscous, unsteady, low-speed flows in complex domains at only a fraction of the computing cost required for the CFD solution of the time-dependent flowfield.

Similar techniques were applied for aeroacoustic computations of higher Mach number flows with appreciable compressibility effects. Sankar et al.[8] assumed that the flowfield variable vector could be decomposed into three components as $q = q_o + q' + q''$, where q_o represents the mean steady flowfield, q'' is an externally imposed acoustic field, and q' is the acoustic field generated in response to the imposed acoustic field. In Ref. 9, the flow variables q were decomposed into a mean flow component q_o and a perturbation component q', as $q = q_o + q'$. This separation into flow and acoustic components was performed to ensure that the mean flow does not overwhelm the acoustic component. The acoustic field in Ref. 9 is computed from a set of inhomogeneous, inviscid equations. The technique of Ref. 9 was used for numerical predictions of jet noise.

Presented as Paper 97-1627 at the AIAA/CEAS 3rd Aeroacoustics Conference, Atlanta, GA, 12–14 May 1997; received 3 October 1997; revision received 22 March 1999; accepted for publication 25 March 1999.

*Senior Research Scientist; currently Senior Research Scientist, Nielsen Engineering and Research, Inc., 526 Clyde Avenue, Mountain View, CA 94043-2212. Associate Fellow AIAA.

The technique of Ref. 7 was applied to the calculation of sound generation by low-speed, practically incompressible flow over a two-dimensional cavity[10] and for the calculation of the sound generated by a corotating vortex pair.[11,12] The governing equations originally presented in Ref. 7 included acoustic and hydrodynamic variable derivatives in a nondivergence form. Therefore, in Refs. 10 and 11, McCormack's predictor corrector scheme was used for the numerical solution because standard explicit and implicit schemes applied to the solution of the compressible Euler equations were not directly applicable. In Ref. 12, the equations for the acoustic field were written in a primitive variable form. The primitive variable form enabled the use of an upwind-biased, high-order numerical scheme for the numerical solution, whereas in Refs. 10 and 11, a scheme that was second-order accurate in space and time was used.

In this paper, the equations governing the sound field, originally proposed by Hardin and Pope, are rewritten into a form similar to the conservative form of the compressible Euler equations, using a simple transformation of variables. The advantage of the new formulation is that the equations are in strong conservation-law form; therefore, high-resolution numerical schemes developed for the solution of the compressible Euler equations are directly applicable. The numerical solution of the transformed equations is obtained with a standard Riemann solver widely used for solution of the inviscid, compressible gasdynamic equations. Numerical solutions are obtained for the same model problem of sound generated by the corotating vortices that was used to test the accuracy of the numerical scheme in Ref. 12. Results obtained with a third- and a fifth-order scheme are presented and compared with the analytic solution.

II. Governing Equations

The essential feature of the Hardin and Pope two-step method is the introduction of a hydrodynamic density correction, $\rho_1 = \rho_1(\boldsymbol{x}, t)$, which is defined as

$$\rho_1 = (P - \bar{P})/c_o^2 \tag{1}$$

with

$$\bar{P} = \lim_{T\to\infty} \frac{1}{T}\int_0^T P \,\mathrm{d}t$$

For isentropic flow the pressure, $p = p' + P$, is related to density through the following algebraic equation:

$$p/p_{\text{ref}} = (\rho/\rho_{\text{ref}})^{\gamma} \tag{2}$$

Incompressible-flow pressure fluctuations, $p_1(\boldsymbol{x}, t)$, are balanced by the density fluctuations, $\rho_1(\boldsymbol{x}, t)$, i.e., $p_1(\boldsymbol{x}, t) = c^2\rho_1(\boldsymbol{x}, t)$. Substituting $\rho = (\rho_o + \rho_1) + \rho'$, $u_i = U_i + u_i'$, and $p = P + p'$ in the compressible-flow equations and utilizing the incompressible-flow equations to eliminate terms involving U_i, P, we obtain a set of first-order nonlinear equations for the acoustic perturbations.

A. Isentropic Flow

The original form of the equations governing the acoustic field, derived in Ref. 7, is

$$\frac{\partial \boldsymbol{Q}}{\partial t} + \frac{\partial \boldsymbol{F}}{\partial x} + \frac{\partial \boldsymbol{G}}{\partial y} = \boldsymbol{S} \tag{3}$$

where $\boldsymbol{Q}$ is a vector that contains both acoustic and hydrodynamic variables. For example, the momentum derivatives include the acoustic density fluctuation ρ' and the sum of momenta with respect to the acoustic velocity $(\rho_o + \rho_1 + \rho')\boldsymbol{u}'$, plus the momentum with respect to the hydrodynamic velocity $\rho'\boldsymbol{U}$. This vector is

$$\boldsymbol{Q} = \begin{Bmatrix} \rho' \\ (\rho_0 + \rho_1 + \rho')u' + \rho' U \\ (\rho_0 + \rho_1 + \rho')v' + \rho' V \end{Bmatrix}$$

The nonlinear convective flux terms $\boldsymbol{F}$ and $\boldsymbol{G}$ are also of mixed type and include both acoustic and hydrodynamic terms. These flux vectors are

$$\boldsymbol{F} = \begin{Bmatrix} (\rho_0 + \rho_1 + \rho')u' + \rho' U \\ (\rho_0 + \rho_1 + \rho')(2Uu' + u'^2) + \rho' U^2 + p' \\ (\rho_0 + \rho_1 + \rho')(Vu' + Uv' + u'v') + \rho' UV \end{Bmatrix}$$

$$\boldsymbol{G} = \begin{Bmatrix} (\rho_0 + \rho_1 + \rho')v' + \rho' V \\ (\rho_0 + \rho_1 + \rho')(Vu' + Uv' + u'v') + \rho' UV \\ (\rho_0 + \rho_1 + \rho')(2Vv' + v'^2) + \rho' V^2 + p' \end{Bmatrix}$$

The source term $\boldsymbol{S}$ includes the total derivatives of the hydrodynamic density correction ρ_1 and its fluxes $\rho_1 U$ and $\rho_1 V$. This term is given by

$$\boldsymbol{S} = -\begin{Bmatrix} \frac{\partial}{\partial t}(\rho_1) + U\frac{\partial}{\partial x}(\rho_1) + V\frac{\partial}{\partial y}(\rho_1) \\ \frac{\partial}{\partial t}(\rho_1 U) + U\frac{\partial}{\partial x}(\rho_1 U) + V\frac{\partial}{\partial y}(\rho_1 U) \\ \frac{\partial}{\partial t}(\rho_1 V) + U\frac{\partial}{\partial x}(\rho_1 V) + V\frac{\partial}{\partial y}(\rho_1 V) \end{Bmatrix} = -\frac{\mathrm{D}}{\mathrm{D}t}\begin{Bmatrix} \rho_1 \\ \rho_1 U \\ \rho_1 V \end{Bmatrix}$$

In Eq. (3), the acoustic density fluctuation ρ' is normalized by ρ_o, the acoustic velocities are normalized by c_o, and the acoustic pressure is normalized by $\rho_o c_o^2$. Therefore, the acoustic pressure for isentropic-flow pressure is obtained as in Eq. (2) from

$$p' = (1/\gamma)(\rho_o + \rho_1 + \rho')^{\gamma} - P$$

The following substitutions of variables are introduced: $\rho = \rho_o + \rho_1 + \rho'$, $\hat{\rho} = \rho_o + \rho_1$, $u = U + u'$, and $v = V + v'$. With these substitutions, the variable vector $\boldsymbol{Q}$ and the flux vectors $\boldsymbol{F}$, $\boldsymbol{G}$ can be rewritten as

$$\boldsymbol{Q} = \begin{Bmatrix} \rho \\ \rho u \\ \rho v \end{Bmatrix} - \begin{Bmatrix} \hat{\rho} \\ \hat{\rho} U \\ \hat{\rho} V \end{Bmatrix} = \boldsymbol{q} - \hat{\boldsymbol{q}}$$

$$\boldsymbol{F} = \begin{Bmatrix} \rho u \\ \rho u^2 + p' \\ \rho uv \end{Bmatrix} - \begin{Bmatrix} \hat{\rho} U \\ \hat{\rho} U^2 \\ \hat{\rho} UV \end{Bmatrix} = \boldsymbol{f} - \hat{\boldsymbol{f}}$$

$$\boldsymbol{G} = \begin{Bmatrix} \rho v \\ \rho vu \\ \rho v^2 + p' \end{Bmatrix} - \begin{Bmatrix} \hat{\rho} V \\ \hat{\rho} VU \\ \hat{\rho} V^2 \end{Bmatrix} = \boldsymbol{g} - \hat{\boldsymbol{g}}$$

The terms $\hat{\boldsymbol{q}}$, $\hat{\boldsymbol{f}}$, and $\hat{\boldsymbol{g}}$ depend only on the incompressible flow velocities, the density correction ρ_1, and the constant incompressible density ρ_o. They are, therefore, source terms and are moved to the right-hand side as additions to the original source term $\boldsymbol{S}$. The left-hand side, however, with the remaining vectors $\boldsymbol{q}$, $\boldsymbol{f}$, and $\boldsymbol{g}$, has a form identical to the continuity and momentum in the compressible Euler equations for the new variables $\rho = \rho_o + \rho_1 + \rho'$, $u = U + u'$, and $v = V + v'$. Thus, the governing equations are rewritten in the following compact form:

$$\frac{\partial \boldsymbol{q}}{\partial t} + \frac{\partial \boldsymbol{f}}{\partial x} + \frac{\partial \boldsymbol{g}}{\partial y} = \frac{\mathrm{D}\boldsymbol{s}}{\mathrm{D}t} \tag{4}$$

where

$$\boldsymbol{s} = \boldsymbol{S} + \hat{\boldsymbol{S}}, \qquad \frac{\mathrm{D}}{\mathrm{D}t} = \frac{\partial}{\partial t} + U\frac{\partial}{\partial x} + V\frac{\partial}{\partial y}, \qquad \boldsymbol{s} = \begin{Bmatrix} \rho_o \\ \rho_o U \\ \rho_o V \end{Bmatrix}$$

as the new source-term vector. The incompressibility condition for the mean flow ($\nabla \cdot \boldsymbol{V} = 0$) yields

$$\frac{\partial \hat{\rho}}{\partial t} + \frac{\partial \hat{\rho} U}{\partial x} + \frac{\partial \hat{\rho} V}{\partial y} = \frac{\mathrm{D}\hat{\rho}}{\mathrm{D}t}$$

$$\frac{\partial \hat{\rho} U}{\partial t} + \frac{\partial \hat{\rho} U^2}{\partial x} + \frac{\partial \hat{\rho} U V}{\partial y} = \frac{\mathrm{D}\hat{\rho} U}{\mathrm{D}t}$$

Therefore, $\hat{\boldsymbol{S}} = \hat{\boldsymbol{q}} + \hat{\boldsymbol{f}} + \hat{\boldsymbol{g}}$ can be written as

$$\hat{\boldsymbol{S}} = \frac{\mathrm{D}}{\mathrm{D}t}(\hat{\rho}, \hat{\rho} U, \hat{\rho} V)^T, \qquad \hat{\rho} = \rho_o + \rho_1$$

The transformed equations are in conservation form and more convenient for numerical implementation. These equations can be solved numerically with standard, high-resolution central-difference or upwind methods used for solution of the compressible Euler equations.

B. Nonisentropic Flow

For nonisentropic flows the energy equation of the compressible-flow equations can be used to compute the acoustic pressure. The acoustic pressure p' is coupled to the internal energy of the acoustic perturbation e' with the following equation of state:

$$p = (P + p') = (\gamma - 1)[e - \rho(u^2 + v^2)/2] \tag{5}$$

where the density and velocities and the total internal energy are sums of the hydrodynamic components plus the acoustic fluctuation as

$$\rho = \rho_o + \rho_1 + \rho'$$

$$u = U + u', \qquad v = V + v', \qquad e = E + e'$$

The internal energy E for incompressible viscous flow is decoupled from continuity and momentum and satisfies the following equation:

$$\rho_o \frac{\mathrm{D}E}{\mathrm{D}t} = \Phi$$

where Φ is the viscous dissipation function

$$\Phi = \mu\left[2\left(\frac{\partial U}{\partial x}\right)^2 + 2\left(\frac{\partial V}{\partial y}\right)^2 + \left(\frac{\partial U}{\partial y} + \frac{\partial V}{\partial x}\right)^2 - \frac{2}{3}\left(\frac{\partial U}{\partial x} + \frac{\partial V}{\partial y}\right)^2\right]$$

for incompressible two-dimensional flow.

The total internal energy $e = E + e'$ for compressible inviscid flow is obtained from

$$(\rho_o + \rho_1 + \rho')\frac{\mathrm{D}e}{\mathrm{D}t} + (P + p')[\nabla \cdot (\boldsymbol{V} + \boldsymbol{v}')] = 0$$

The energy equation for the acoustic perturbations is similar to the energy equation for the compressible inviscid flow:

$$\frac{\partial e}{\partial t} + \frac{\partial}{\partial x}[u(e + p')] + \frac{\partial}{\partial y}[v(e + p')] = \frac{\partial u P}{\partial x} + \frac{\partial v P}{\partial y} \tag{6}$$

This is an inhomogeneous equation in conservation form for the internal energy fluctuations. Addition of Eq. (6) to Eqs. (4) yields a system of four equations for the computation of sound generated by nonisentropic flows. Equation (6) includes acoustic viscous losses whereas the density correction ρ_1 is still assumed to be isentropic. The left-hand side of the equations governing the acoustic disturbances for nonisentropic flows, given in Appendix A, has the same form as the compressible, inviscid-flow equations. Therefore, standard, inviscid compressible codes can be used for solution of the acoustic equations, with minor modifications.

III. Numerical Implementation

A. Time Integration

Time marching is obtained with a fourth-order Runge–Kutta method[13]:

$$q^0 = q^{(n)}, \qquad q^1 = q^0 + c_1 \mathcal{R}(q^0), \qquad q^2 = q^0 + c_2 \mathcal{R}(q^1)$$

$$q^3 = q^0 + c_3 \mathcal{R}(q^2), \qquad q^4 = q^0 + c_4 \mathcal{R}(q^3), \qquad q^{(n+1)} = q^4 \tag{7}$$

where $\boldsymbol{q}$ is the solution vector and $\mathcal{R}$ is the right-hand-side residual term.

Implicit time-marching schemes implemented for the compressible Euler equations can be used for implicit time integration of Eqs. (4). In most applications[7,10] the numerical mesh used for the aeroacoustic computations has a considerably larger grid spacing than the grid used to obtain the CFD solution of the viscous incompressible flow. Therefore, explicit Runge–Kutta time integration methods that are not diffusive, have good wave propagation properties, and allow large time steps are quite suitable for the aeroacoustic calculations. In this paper, only an explicit time integration scheme is used.

B. Space Discretization

Space discretization of the divergence form of the governing equations can be achieved with standard central-difference schemes[13] that require addition of artificial dissipation or compact schemes.[14,15] Upwind schemes, such as flux-vector splitting[16,17] and approximate Riemann solvers[18,19] developed for the numerical solution of nonlinear hyperbolic equations, also can be used. In either case, high-order space discretization is required to accomplish propagation of the acoustic disturbances with correct amplitude and phase using the smallest possible number of grid points per wavelength. The following one-dimensional upwind scheme based on Roe's[18] flux-difference splitting, originally developed as an approximate Riemann solver for the compressible gasdynamic equations, is used for evaluation of the inviscid flux terms. Flux-difference splitting of the convective terms of the governing equations (4) is performed on the basis of the sign of eigenvalues of the flux Jacobian matrix $A = \partial \boldsymbol{f}/\partial \boldsymbol{q}$ of the flux vectors.

Roe's flux-difference splitting approximates the convective flux derivative by

$$\frac{\partial \hat{f}}{\partial x} \approx \frac{\tilde{F}_{i+\frac{1}{2}} - \tilde{F}_{i-\frac{1}{2}}}{\Delta x} \tag{8}$$

where $\tilde{F}_{i+1/2}$ is a numerical flux given by

$$\tilde{F}_{i+\frac{1}{2}} = \tfrac{1}{2}\left[\hat{F}(q_{i+1}) + \hat{F}(q_i) - \phi_{i+\frac{1}{2}}\right] \tag{9}$$

In Eq. (9), the first two terms yield the second-order, central-difference scheme and the term $\phi_{i+1/2}$ represents an upwinding dissipative term, depending on the flux difference of the positive and negative traveling waves. First-order upwinding is obtained by

$$\phi_{i+\frac{1}{2}} = \Delta F^+_{i+\frac{1}{2}} - \Delta F^-_{i+\frac{1}{2}} \tag{10}$$

In practice, a first-order scheme is too diffusive to allow solutions with a reasonable number of grid points. Therefore, the following third- and fifth-order schemes are used. The third-order-accurate scheme is obtained when the term $\phi_{i+1/2}$ is computed as

$$\phi_{i+\frac{1}{2}} = -\tfrac{1}{3}\left[\Delta F^+_{i-\frac{1}{2}} - \Delta F^+_{i+\frac{1}{2}} + \Delta F^-_{i+\frac{1}{2}} - \Delta F^-_{i+\frac{3}{2}}\right] \tag{11}$$

and the fifth-order-accurate scheme is obtained for

$$\phi_{i+\frac{1}{2}} = -\tfrac{1}{30}\Big[-2\Delta F^+_{i-\frac{3}{2}} + 11\Delta F^+_{i-\frac{1}{2}} - 6\Delta F^+_{i+\frac{1}{2}} - 3\Delta F^+_{i+\frac{3}{2}} + 2\Delta F^-_{i+\frac{5}{2}} - 11\Delta F^-_{i+\frac{3}{2}} + 6\Delta F^-_{i+\frac{1}{2}} + 3\Delta F^-_{i-\frac{1}{2}}\Big] \tag{12}$$

The flux differences $\Delta F^{\pm}_{i+1/2}$ are computed as follows:

$$\Delta F^{\pm}_{i+\frac{1}{2}} = A^{\pm}(\bar{q}) \times (q_{i+1} - q_i) \tag{13}$$

where $\bar{q}$ contains the Roe average variables, given by

$$\bar{\rho} = \sqrt{\rho_{i+1}} + \sqrt{\rho_i}, \qquad \bar{u} = \frac{u_{i+1}\sqrt{\rho_{i+1}} + u_i\sqrt{\rho_i}}{\bar{\rho}}$$

$$\bar{v} = \frac{v_{i+1}\sqrt{\rho_{i+1}} + v_i\sqrt{\rho_i}}{\bar{\rho}} \tag{14}$$

and A^+, A^- are the parts of the flux Jacobian matrix with only positive and only negative eigenvalues, respectively:

$$A^{\pm} = X\Lambda^{\pm}X^{-1} \tag{15}$$

where X and X^{-1} are the right and left eigenvectors of the flux Jacobian matrix and $\Lambda^{\pm}$ is a diagonal matrix containing both positive and negative eigenvalues on the main diagonal. The flux Jacobian matrices and X, Λ, and X^{-1} are given in Appendix B.

C. Boundary Conditions

At the far field of the computational domain, the Tam–Webb[3] acoustic radiation boundary condition is applied, and the acoustic variables are obtained as follows:

$$\left[\frac{1}{(V_r + c)}\frac{\partial}{\partial t} + \cos\theta\frac{\partial}{\partial x} + \sin\theta\frac{\partial}{\partial y} + \frac{1}{2r}\right]\cdot \boldsymbol{q}_b = 0 \tag{16}$$

where $\boldsymbol{q}_b = (\rho' + \rho_1, u', v')^T$ and $V_r = (U + u')\cos\theta + (V + v')\sin\theta$, $r = \sqrt{(x^2 + y^2)}$, and θ represents the polar angle between the boundary point and the source location, which is usually at the origin of the coordinate system. The time derivative is discretized with a first-order-accurate formula, and the computational boundaries are updated explicitly. A systematic comparison of different boundary conditions for aeroacoustics was performed in Ref. 4. It was found that the Tam–Webb radiation boundary conditions yield the best results. For more complex problems, with moving acoustic sources, numerical boundary treatment can be obtained as suggested by Hu.[20]

IV. Results

Computation of the sound field generated by low-speed flow with the Hardin and Pope two-step approach requires accurate long-time integration of the incompressible, unsteady flowfield, so that meaningful time averages for the definition of the perturbation density ρ_1 can be obtained. Viscous flowfields must be computed on a numerical mesh different from the mesh required for the aeroacoustic computation. For example, high resolution near the solid boundaries is not needed for the aeroacoustic computations. On the other hand, a rather uniform mesh with very little stretching and approximately the same number of points per wavelength is required for the aeroacoustic calculations. Therefore, the incompressible-flow variables must be interpolated on the numerical mesh used for the aeroacoustic computation. In addition, for most practical problems the Reynolds number is high enough and a turbulent flow calculation is needed. Application of a turbulence model introduces additional uncertainties in the flowfield computation that eventually affect the aeroacoustic calculations. As a result, testing of numerical methods for the equations governing the aeroacoustics can be time-consuming for complex flowfields. The Hardin–Pope technique was applied for the computation of sound generation from a corotating vortex pair.[11,12] For this problem, both the incompressible flowfield and the sound field[21,22] have a closed-form solution. This model problem was used to evaluate the accuracy of the numerical scheme in Ref. 12. In this paper, testing of the numerical solution of the equations governing the acoustics is performed for the same model problem. Computed results are compared with the closed-form solution. The solution for the corotating vortex pair obtained in Ref. 21 with the method of matched asymptotic expansions (MAE) is used.

The corotating vortex pair consists of two point vortices that are separated by a fixed distance. A schematic of the corotating vortices is shown in Fig. 1. These vortices rotate around each other with a period $T = 8\pi^2 R_o^2/\Gamma$. The half distance between the vortex centers is denoted R_o, and Γ is the vortex circulation.

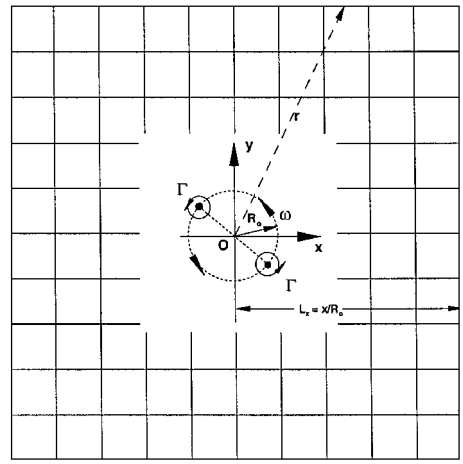

Fig. 1 Schematic of corotating vortices and the far-field Cartesian mesh.

The inherent unsteadiness of the flowfield of the corotating vortices generates sound. Each vortex induces on the other a velocity $v_\theta = \Gamma/4\pi R_o$. A rotating Mach number is defined from v_θ as $M_r = v_\theta/c_o = \Gamma/(4\pi R_o c_o) = 2\pi R_o/Tc_o$, where c_o is the freestream speed of sound. The flowfield is obtained from a complex potential function, and the incompressible-flow velocities, the hydrodynamic pressure, and the acoustic pressure fluctuation are given by

$$U - iV = \frac{\Gamma}{i\pi}\frac{z}{z^2 - b^2}$$

$$P = P_o + \rho_o\frac{\Gamma\omega}{\pi}\left[\text{Real}\left(\frac{b^2}{z^2 - b^2}\right) - \frac{\Gamma r}{2\pi\omega Z_b}\right]$$

$$P_{\text{av}} = P_o - \rho_o\frac{\Gamma^2}{2\pi^2}\frac{r^2}{r^4 - R_o^4}$$

$$p' = p'_A[J_2(kr)\cos(\Psi) - Y_2(kr)\sin(\Psi)]$$

$$p'_A = \frac{\rho_o\Gamma^4}{64\pi^3 R_o^4 c_o^2}, \qquad \Psi = 2(\omega t - \theta)$$

where $z = x + iy = re^{i\theta}$, $b = R_o e^{i\omega t}$, $\omega = \Gamma/4\pi R_o^2$ is the angular speed, $Z_b = \sqrt{(z^2 - b^2)}$, $k = 2\omega/c_o$, and $J_2(kr)$, $Y_2(kr)$ are the second-order Bessel functions of the first and second kind, respectively. The vortex sound theory proposed by Möhring[22] also was used to predict sound from acoustically compact vortical flows. Application of this theory[1] yielded a quadrupole expression for the acoustic pressure equivalent to the one derived in Ref. 21 with the MAE solution.

The strength of the vortices is proportional to the circulation Γ, which also determines M_r and the intensity and frequency of the acoustic field. At middle distance between the point vortices, which is the coordinate system origin, the acoustic pressure p' becomes singular, and it is very large close to the vortex centers. In this region, the hydrodynamic velocities and pressure have steep and large gradients. In Ref. 11, a vortex core model was used to replace the point vortices. The vortex core model is not used in this paper; instead, the mesh points are placed far enough from the vortex centers. However, numerical solutions on grids with nodes located closer than the point vortices' half-separation distance R_o could not obtain convergence.

An equally spaced Cartesian grid is used for the numerical solution. A schematic of the mesh with the vortices is shown in Fig. 1. The computational domain is centered at the origin, where the source is located. The grid has the same number of grid points from the origin to the far-field boundaries. All solutions are computed for $M_r = 0.05, \Gamma = 2\pi/10$. Grid spacing of $\Delta x = 4R_o$, where $R_o = 1$ because it is used as reference length, provides approximately 16 points per wavelength. A coarser grid solution, $\Delta x = 6$, provides 12 points per wavelength. The acoustic field computation starts from zero values of acoustic density and velocity fluctuations. Acoustic waves are generated initially at the origin, where the incompressible-flow

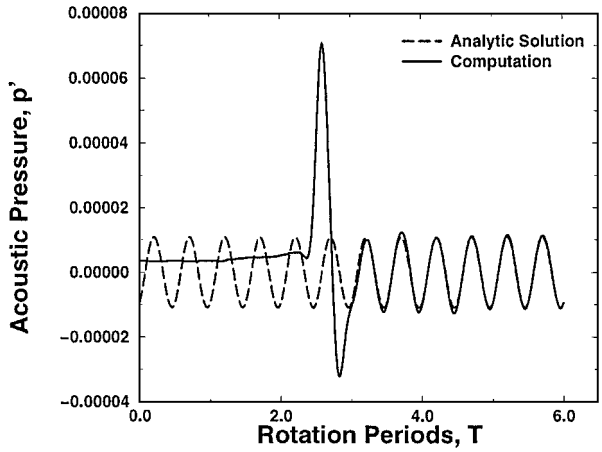

Fig. 2 Time evolution of the acoustic pressure obtained by the third-order-accurate scheme at $x = 220$, $y = 0$ ($\Delta t = 0.62$, $\Delta x = 4$, $M_r = 0.05$, $\Gamma = 2\pi/10$).

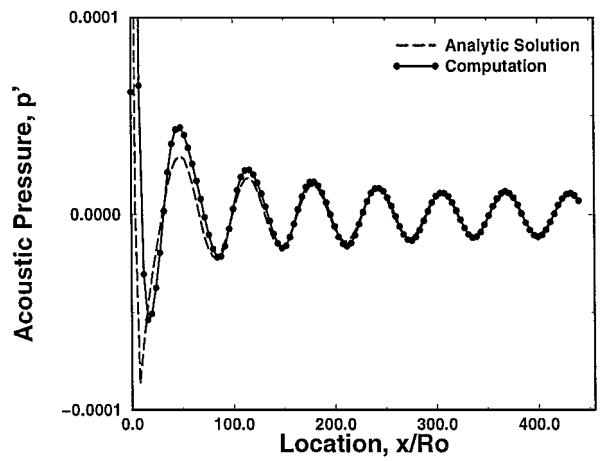

Fig. 3 Comparison of acoustic pressure obtained by the third-order-accurate scheme with the analytic solution, along the horizontal direction ($\Delta t = 0.62$, $\Delta x = 4$, $M_r = 0.05$, $\Gamma = 2\pi/10$).

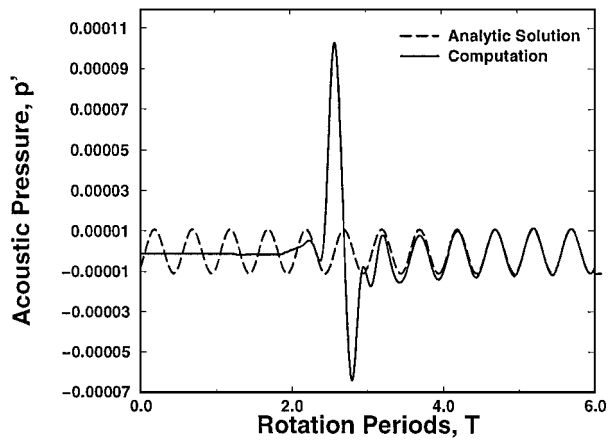

Fig. 4 Time evolution of acoustic pressure obtained by the fifth-order-accurate scheme at $x = 220$, $y = 0$ ($\Delta t = 0.62$, $\Delta x = 6$, $M_r = 0.05$, $\Gamma = 2\pi/10$).

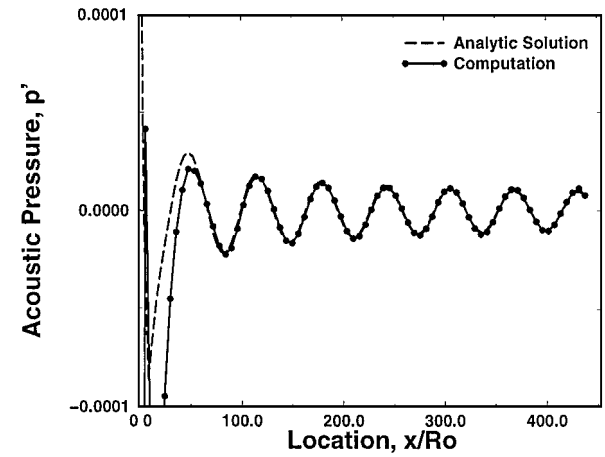

Fig. 5 Comparison of the computed acoustic pressure obtained by the fifth-order-accurate scheme with the analytic solution, along the horizontal direction ($\Delta t = 0.62$, $\Delta x = 6$, $M_r = 0.05$, $\Gamma = 2\pi/10$).

gradients are the largest. As the unsteady computation progresses, these waves propagate outward to the computational boundaries at a rate approximately one wavelength per cycle. The solution reaches time periodicity, when the waves formed at startup are convected outside of the domain. Depending on the size of the computational domain, approximately five cycles are required to achieve time periodic response. Most solutions were obtained for computational domains extending 420 nondimensional units x/R_o away from the source at all directions. Numerical solutions obtained in larger domains have not shown differences.

The time evolution of the computed acoustic pressure, described in the preceding paragraph, is shown in Fig. 2 for a point $x = 220$ on the horizontal axis. These results are computed with the third-order accurate scheme of Eq. (11) and a grid spacing $\Delta x = 4$. In Fig. 2, the computed acoustic pressure at half distance between the source and the outer boundary along the horizontal direction is compared with the analytic solution. After the transients are removed, the computed acoustic-pressure time variation is in close agreement with the analytic solution. The spatial variation of the computed acoustic pressure along the horizontal from the source to the outer boundary is compared with the analytic solution in Fig. 3. Close to the vortices the computation shows only qualitative agreement with the analytic solution. There is good agreement, however, for the locations away from the vortices. The same agreement in both spatial and time variation was obtained along the diagonal direction for a line inclined at an angle of 45 deg to the horizontal axis.

In Fig. 4, the time variation of the computed acoustic pressure, for the same location as in Fig. 2, $x = 220$, is compared with the analytic solution. The solution shown in Fig. 4 was computed with $\Delta x = 6$ and the fifth-order-accurate scheme of Eq. (12). The fifth-order-accurate computation with grid spacing $\Delta x = 6$ yields essentially the same resolution with the solution obtained with a third-order-accurate scheme and $\Delta x = 4$. The spatial agreement of the fifth-order-accurate computation with the analytic solution along the horizontal direction is shown in Fig. 5. In spite of the reduced grid spacing, the spatial agreement of the computed solution with the analytic results does not deteriorate. Detailed comparisons of the third- and fifth-order-accurate solutions with the analytic solution are shown in Figs. 6 and 7. The time variation of the acoustic pressure computed with the third- and fifth-order-accurate solutions is compared to the analytic solution in Fig. 6. The space resolution of these solutions is shown in Fig. 7. It is seen in Figs. 3 and 5 that, in the region close to the vortex centers, there are discrepancies from the analytic solution. Therefore, the comparison in Fig. 7 is performed for the far field only. It is observed that the fifth-order-accurate numerical solution shows a better agreement with the analytic results even though it was computed with a larger grid spacing.

The fifth-order-accurate solution is obtained only at a small increase of the cost needed to compute the third-order-accurate results. The comparisons of Figs. 6 and 7 indicate that the fifth-order-accurate method yields savings of approximately 50% for essentially the same solution quality. The computing cost of the present method is comparable to the cost of the upwind-biased scheme of Ref. 12, which utilizes a decomposition of the Jacobian matrix similar to the present decomposition given in Appendix B. A typical computation requires 15 min of CPU time on a single-processor of a Silicon Graphics, Inc. (SGI), work station. The advantage of the present approach is that the fully conservative formulation is more

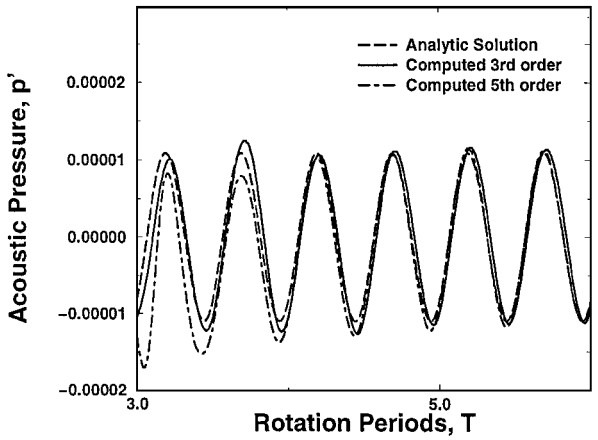

Fig. 6 Effect of order of accuracy on time resolution of the solutions computed with the third-order scheme and $\Delta x = 4$, and with the fifth-order scheme and $\Delta x = 6$.

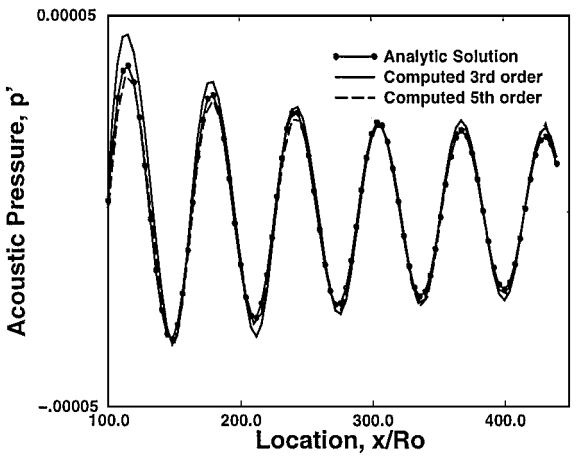

Fig. 7 Effect of order of accuracy on space resolution of the solutions computed with the third-order scheme and $\Delta x = 4$, and with the fifth-order scheme and $\Delta x = 6$.

appropriate for numerical solution of problems that involve nonlinear wave steepening, such as the pulsating sphere problem at high Mach numbers, which is discussed in Ref. 7. Another advantage of the present method is that widely available time-accurate, high-resolution solvers for the compressible Euler equations can be used for numerical solutions with the conservative form.

V. Conclusions

The equations governing generation and propagation of aeroacoustic disturbances caused by unsteady, low-speed flow have been rewritten for new variables in a divergence form. This form is similar to the strong conservation-law form of compressible Euler equations. An upwind-biased numerical scheme based on flux-difference splitting of the convective flux vectors was applied to the numerical solution of these equations. Results have been obtained for a sample problem of a corotating vortex pair that does not require time-accurate, incompressible-flowfield CFD solutions that are CPU intensive. The numerical solution for the radiated sound was in good agreement with the analytic solution. It was shown that computation with a high-order-accurate scheme yields essentially the same accuracy as the lower-order scheme with smaller grid spacing.

Appendix A: Equations for Nonisentropic Flows

The equations governing aeroacoustic disturbances for nonisentropic flows are

$$\frac{\partial \boldsymbol{q}}{\partial t} + \frac{\partial \boldsymbol{f}}{\partial x} + \frac{\partial \boldsymbol{g}}{\partial y} = \frac{\mathrm{D}\boldsymbol{s}}{\mathrm{D}t}$$

where $\boldsymbol{q}$, $\boldsymbol{f}$, $\boldsymbol{g}$, and $\boldsymbol{s}$ are given by

$$\boldsymbol{q} = \begin{Bmatrix} \rho \\ \rho u \\ \rho v \\ e \end{Bmatrix}, \qquad \boldsymbol{f} = \begin{Bmatrix} \rho u \\ \rho u^2 + p' \\ \rho uv \\ u(e+p) \end{Bmatrix}, \qquad \boldsymbol{g} = \begin{Bmatrix} \rho v \\ \rho vu \\ \rho v^2 + p' \\ v(e+p) \end{Bmatrix}$$

where $e = E + e'$ and E is obtained from the viscous, incompressible flow solution, and

$$\hat{\boldsymbol{S}} = \frac{\mathrm{D}}{\mathrm{D}t}(\hat{\rho}, \hat{\rho}U, \hat{\rho}V, 0)^T$$

Appendix B: Eigenvalue and Eigenvector Matrices

The flux Jacobian matrix $A = \partial \boldsymbol{f}/\partial \boldsymbol{q}$ can be obtained from the primitive variable flux Jacobian $A' = \partial \boldsymbol{F}'/\partial \boldsymbol{q}'$ and the transformation matrix $P = \partial \boldsymbol{q}/\partial \boldsymbol{q}'$, where $\boldsymbol{q}$ is the conservative variable vector $\boldsymbol{q} = [\rho, \rho u, \rho v]^T$ and $\boldsymbol{q}'$ is the primitive variable vector $\boldsymbol{q} = [\rho', u', v']^T$.

The conservative variable flux Jacobian matrices A, B are given by

$$[A] = \frac{\partial \boldsymbol{f}}{\partial \boldsymbol{q}} = \begin{bmatrix} 0 & 1 & 0 \\ c^2 - u^2 & 2u & 0 \\ -(uv) & v & u \end{bmatrix}$$

$$[B] = \frac{\partial \boldsymbol{g}}{\partial \boldsymbol{q}} = \begin{bmatrix} 0 & 0 & 1 \\ -(uv) & v & u \\ c^2 - v^2 & 0 & 2v \end{bmatrix}$$

where c is the local speed of sound $c^2 = \partial p'/\partial \rho$.

The matrices $X\Lambda$ and X^{-1} are given by

$$\Lambda_A = \begin{bmatrix} u & 0 & 0 \\ 0 & u-c & 0 \\ 0 & 0 & c+u \end{bmatrix}, \qquad \Lambda_B = \begin{bmatrix} v & 0 & 0 \\ 0 & v-c & 0 \\ 0 & 0 & v+u \end{bmatrix}$$

$$X_A = \begin{bmatrix} 0 & 1 & 1 \\ 0 & (u-c) & (u+c) \\ v & v & v \end{bmatrix}$$

$$X_B = \begin{bmatrix} 0 & 1 & 1 \\ u & u & u \\ 0 & (v-c) & (v+c) \end{bmatrix}$$

$$X_A^{-1} = \begin{bmatrix} -1 & 0 & 1/v \\ (c+u)/2c & -1/2c & 0 \\ (c-u)/2c & 1/2c & 0 \end{bmatrix}$$

$$X_B^{-1} = \begin{bmatrix} -1 & 1/u & 0 \\ (v+c)/2c & 0 & -1/2c \\ (c-v)/2c & 0 & 1/2c \end{bmatrix}$$

The matrices $X\Lambda$ and X^{-1} have very simple structure. Also, the flux Jacobians and the eigenvalues are of the same form in the transformed and in the original set of equations.

References

[1] Michell, B. E., Lele, S. K., and Moin, P., "Direct Computation of Sound from a Compressible Co-Rotating Vortex Pair," *Journal of Fluid Mechanics*, Vol. 285, 1995, pp. 181–202.

[2] Wang, M., Lele, S. K., and Moin, P., "Computation of Quadrupole Noise Using Acoustic Analogy," *AIAA Journal*, Vol. 34, No. 11, 1996, pp. 2247–2254.

[3] Tam, C. K., and Webb, J. C., "Dispersion–Relation–Preserving Schemes for Computational Aeroacoustics," *Journal of Computational Physics*, Vol. 107, No. 2, 1993, pp. 262–281.

[4] Hixon, R., Shih, S.-H., and Mankbadi, R. R., "Valuation of Boundary Conditions for Computational Aeroacoustics," *AIAA Journal*, Vol. 33, No. 11, 1995, pp. 2006–2012.

[5]Lighthill, M. J., "On Sound Generated Aerodynamically, I. General Theory," *Proceedings of the Royal Society of London, Series A: Mathematical and Physical Sciences*, Vol. 211, 1952, pp. 564–587.

[6]Lyrintzis, A. S., "Review: The Use of Kirchhoff's Method in Computational Aeroacoustics," *Journal of Fluids Engineering*, Vol. 116, No. 4, 1994, pp. 665–676.

[7]Hardin, J. C., and Pope, S. D., "An Acoustic/Viscous Splitting Technique for Computational Aeroacoustics," *Theoretical and Computational Fluid Dynamics*, Vol. 6, No. 5–6, 1994, pp. 334–340.

[8]Sankar, L. N., Reddy, N. N., and Hariharan, N., "A Third Order Upwind Scheme for Aeroacoustic Applications," AIAA Paper 93-0149, Jan. 1993.

[9]Viswanathan, K., and Sankar, L. N., "Toward the Direct Calculation of Noise: Fluid/Acoustic Coupled Simulation," *AIAA Journal*, Vol. 33, No. 12, 1995, pp. 2271–2279.

[10]Hardin, J. C., and Pope, D. S., "Sound Generation by Flow over a Two-Dimensional Cavity," *AIAA Journal*, Vol. 33, No. 3, 1995, pp. 407–412.

[11]Lee, D. J., and Koo, S. O., "Numerical Study of Sound Generation Due to a Spinning Vortex Pair," *AIAA Journal*, Vol. 33, No. 1, 1995, pp. 20–26.

[12]Ekaterinaris, J. A., "An Upwind Scheme for the Computation of Acoustic Fields Generated by Incompressible Flow," *AIAA Journal*, Vol. 35, No. 9, 1997, pp. 1448–1455.

[13]Jameson, A., Schmidt, W., and Turkel, E., "Numerical Simulations of the Euler Equations by Finite Volume Methods Using Runge–Kutta Time Stepping Schemes," AIAA Paper 81-1259, June 1981.

[14]Lele, S. K., "Compact Finite Difference Schemes with Spectral-Like Resolution," *Journal of Computataional Physics*, Vol. 103, No. 1, 1992, pp. 16–42.

[15]Deng, X., and Maekawa, H., "Compact High-Order Accurate Nonlinear Schemes," *Journal of Computational Physics*, Vol. 130, No. 2, 1997, pp. 77–91.

[16]Steger, J. L., and Warming, R. F., "Flux Vector Splitting of the Inviscid Gas-Dynamic Equations with Applications to Finite Difference Methods," *Journal of Computational Physics*, Vol. 40, No. 2, 1981, pp. 263–293.

[17]Van Leer, B., "Flux Vector Splitting for the Euler Equations," *Proceedings of the 8th International Conference on Numerical Methods in Fluid Dynamics*, edited by E. Krause, Vol. 170, Springer–Verlag, Berlin, 1982, pp. 507–512.

[18]Roe, P. L., "Approximate Riemann Solvers, Parameter Vectors, and Difference Schemes," *Journal of Computational Physics*, Vol. 43, No. 2, 1981, pp. 357–372.

[19]Osher, S., "Riemann Solvers, the Entropy Condition and Difference Approximations," *SIAM Journal on Numerical Analysis*, Vol. 21, No. 2, 1984, pp. 217–235.

[20]Hu, F. Q., "On Absorbing Boundary Conditions for Linearized Euler Equations by a Perfectly Matched Layer," *Journal of Computational Physics*, Vol. 129, No. 1, 1996, pp. 201–219.

[21]Müller, E.-A., and Obermeier, F., "The Spinning Vortices as a Source of Sound," *Fluid Dynamics of Rotor and Fan Supported Aircraft at Subsonic Speeds*, CP-22, AGARD, 1967, pp. 22.1–22.8.

[22]Möhring, W., "On Vortex Sound at Low Mach Number," *Journal of Fluid Mechanics*, Vol. 85, 1978, pp. 685–691.

D. S. McRae
Associate Editor